Optics Letters

Observation of diffraction pattern in two-dimensional optically induced atomic lattice

Jinpeng Yuan,[1,2] Chaohua Wu,[1,2] Lirong Wang,[1,2,*] Gang Chen,[1,2,3] and Suotang Jia[1,2]

[1]State Key Laboratory of Quantum Optics and Quantum Optics Devices, Institute of Laser Spectroscopy, Shanxi University, Taiyuan 030006, China
[2]Collaborative Innovation Center of Extreme Optics, Shanxi University, Taiyuan 030006, China
[3]e-mail: chengang971@163.com
*Corresponding author: wlr@sxu.edu.cn

Received 24 July 2019; accepted 28 July 2019; posted 30 July 2019 (Doc. ID 373617); published 21 August 2019

The diffraction pattern of a two-dimensional optically induced atomic lattice is reported experimentally in a three-level atomic system. Such a two-dimensional optical lattice is established by two orthogonal standing-wave fields induced by the interference of two pairs of coupling laser beams. When the probe beam is launched into it, a spatially modulated discrete diffraction pattern can be obtained at the output plane of the vapor cell under the electromagnetically induced transparency condition. We investigate the diffraction pattern under different experimental parameters and find that it can be effectively controlled by tuning the coupling laser power and two-photon detuning. Our work may potentially pave the way for studying the control of light and other intriguing physical phenomena based on such a periodically modulated atomic lattice.

https://doi.org/10.1364/OL.44.004123

In the past few decades, artificial periodic dielectric structures, such as photonic crystals [1] and waveguides [2,3], have attracted enormous interest due to their unprecedented capacities of engineering the transmission and reflection properties of waves. Such periodic structures provide a powerful tool for control of the fundamental aspects of light propagation, hold an immense potential to design and realize new optical devices [4–6], as well as explore novel topological photonics [7,8]. In addition to studying optical analogs of many fundamental quantum mechanical effects [2], a number of intriguing physical effects, such as controlling spontaneous and thermal emission [9,10], localization of light [11], optical lattice solitons [12], and photon–atom bound state [13] have also been predicted. Nevertheless, the photonic band properties in conventional solid materials are hard to adjust once the periodic dielectric structures are formed, which limits their further investigation and application. As a result, it is necessary and important to experimentally achieve artificial periodic structures with tunable optical properties [14,15].

A coherently prepared multilevel atomic medium may be a qualified candidate because of its easy reconfiguration, flexible tunability, and especially the various coherence control techniques enabled by electromagnetically induced transparency (EIT) [16]. Applying a standing-wave field in an EIT medium, the absorption and dispersion of the probe field may become spatially periodic, and the atomic medium acts as a grating, which is called electromagnetically induced grating or lattice [17]. Compared with traditional periodic structures, such as atomic density gratings [18], such an induced nonmaterial lattice is established by interfering laser beams, and consequently the optical response of the weak probe field to the atomic medium becomes periodically modulated. Recently, one-dimensional optically induced atomic lattices have been experimentally demonstrated [19–23]. In fact, two-dimension (2D) optical lattices play a crucial role in exploring exotic physical phenomena and implementing quantum information, such as topological phase transition [24], chiral edge currents [25], photonic Floquet topological insulators [26,27], topological defects [28], solitons [29,30], and so on. However, the experimental realization of 2D optically induced atomic lattices has not been achieved yet.

In this Letter, we report the experimental realization of such a 2D optically induced atomic lattice in a three-level ^{85}Rb atomic medium under the EIT condition. Such induced 2D lattices are established by the interference of two pairs of coupling fields with the same frequency, and a probe beam is launched into it. As a result, a 2D discrete diffraction pattern can be obtained at the output plane of the vapor cell, reflecting the formation of the spatially modulated susceptibility of the probe beam inside the atomic medium. We also show that the diffraction pattern can be effectively manipulated and optimized by controlling the experimental parameters such as intensity of the coupling laser and two-photon detuning. Our work provides a fertile platform to study the control of light and explore exotic physical phenomena based on such 2D periodically modulated atomic lattices.

Figure 1(a) schematically depicts the experiment setup in a three-level cascade-type ^{85}Rb atomic configuration, which involves a ground state $5S_{1/2}$ ($|1\rangle$), metastable state $5P_{3/2}$ ($|2\rangle$), and excited state $5D_{5/2}$ ($|3\rangle$) [Fig. 1(b)]. The coupling beam (with wavelength $\lambda_c = 776$ nm and frequency ω_c) is obtained from a diode laser (DL1) and can be detuned by

an acousto-optical modulator in a double-pass configuration. It is split into horizontally and vertically polarized beams by a polarization beam splitter (PBS2). The horizontally polarized beam is used as the coupling beam for setting an EIT reference signal, while the vertically polarized beam is transformed into an elliptical profile by an anamorphic prism pair. After passing through PBS5, this elliptically shaped coupling beam is split into two beams with the same intensities and spatial shapes. To construct a 2D periodic modulated optical field, each beam is split into two beams with a small angle after experiencing the standing-wave (SW) configuration [see the black box in Fig. 1(a)]. These four beams (with amplitude E_c and Rabi frequency Ω_c for each beam) recombine at the beam splitter (BS5) and propagate toward a rubidium vapor cell along the z direction, driving the transition $|2\rangle \rightarrow |3\rangle$. Figure 1(c1) shows the configuration of the lasers inside the cell. Two coupling beams in the x–z plane being symmetrically placed with respect to the z axis are incident upon the atomic sample at a small angle 2θ [Fig. 1(c2)]. Its intersection generates a standing wave along the x direction within the atomic ensemble. In the same way, the intersection of another two coupling beams, which is formed at $2\theta'$ in the y–z plane, generates a standing wave along the y direction [Fig. 1(c3)]. That is to say, these four coupling beams induce an effective 2D periodic modulated optical field in the x–y plane [Fig. 1(c4)]. In the experiment, we take $\theta \approx \theta' \approx 0.2°$ for convenience. Thus, the spatial periodicity of the coupling lattices is $d_{x(y)} = \lambda_c/(2 \sin \theta) \approx 110$ μm. When the weak Gaussian probe beam (with wavelength $\lambda_p = 780$ nm, frequency ω_p, Rabi frequency Ω_p, and amplitude E_p) connecting the transition $|1\rangle \rightarrow |2\rangle$ counter-propagates through this coupling lattice, it experiences a spatially modulated index of refraction during propagation under the EIT condition. A discrete diffraction pattern can be observed at the output plane of the cell by a charge-coupled device camera. The 10 cm long atomic vapor cell is wrapped with μ-metal sheets to shield the magnetic field and is heated in an oven.

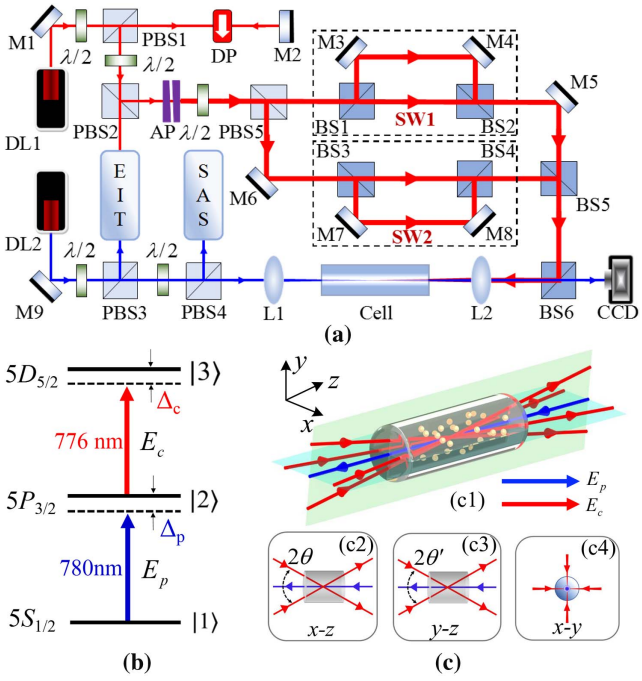

Fig. 1. (a) Sketch of the experimental setup. DL, diode laser; PBS, polarization beam splitter; $\lambda/2$, half-wave plate; L, lens; DP, double-pass configuration; SW, standing-wave configuration; M, high-reflection mirror; AP, anamorphic prism; BS, beam splitter; SAS, saturation absorption spectroscopy; CCD, charge-coupled device. (b) Cascade-type energy-level configuration in the ^{85}Rb atomic vapor and their transitions. The probe beam E_p is applied to drive the 5 $S_{1/2}(|1\rangle) \rightarrow 5P_{3/2}(|2\rangle)$ transition with the detuning Δ_p, while the coupling beam E_c governs the 5 $P_{3/2}(|2\rangle) \rightarrow 5D_{5/2}(|3\rangle)$ transition with the detuning Δ_c. (c) Configuration of the lasers for generating a 2D optically induced lattice inside the vapor cell.

The key point of the experiment is to periodically modulate the refractive index experienced by the probe beam. Before proceeding, we present a theoretical analysis on how to construct this refractive index. With the EIT condition satisfied, the atomic medium modifies the transmission and dispersion profiles of the weak probe beam. As shown in Fig. 1(c), an effective periodic coupling field is generated by two orthogonal standing-wave fields with the same frequency, and its effective Rabi frequency can be written as $|\Omega_{\text{eff}}(x,y)|^2 = 4|\Omega_c|^2 [|\cos(\pi x/d_x)|^2 + |\cos(\pi y/d_y)|^2]$ [31]. The Rabi frequency is defined as $\Omega_c = \mu_{32}E_c/\hbar$, where μ_{ij} is the transition dipole momentum between the levels $|i\rangle$ and $|j\rangle$. The susceptibility, which is associated with the optical properties (specifically the dispersion and absorption of the probe laser) of the atomic medium can be written as $\chi = 2N\mu_{21}\rho_{21}/(\varepsilon_0 E_p)$, where N is the atomic ensemble density, ε_0 is the vacuum dielectric constant [32], and ρ_{21} is the density-matrix element for the transition $|1\rangle \rightarrow |2\rangle$. By utilizing the density-matrix method [16], the spatially modulated susceptibility can be given by [31]

$$\chi = \frac{iN|\mu_{21}|^2}{\hbar\varepsilon_0}\left[\gamma_{21} - i\Delta_p + \frac{|\Omega_{\text{eff}}(x,y)|^2/4}{\gamma_{32} - i(\Delta_p - \Delta_c)}\right]^{-1}, \quad (1)$$

where γ_{ij} is the coherence decay rate between $|i\rangle$ and $|j\rangle$, and $\Delta_p = \omega_p - \omega_{21}$ and $\Delta_c = \omega_{32} - \omega_c$ are detunings of the probe and coupling field, respectively. Equation (1) shows that when the intensity of the effective coupling field has an amplitude and space modulation [Fig. 2(a)], the susceptibility can be periodically modulated. To illustrate this point explicitly, in Figs. 2(b) and 2(c), we plot the optical properties of the probe beam at the nodes and antinodes of the optically induced lattice. From the absorption curve (see the blue solid lines in these figures), it is found that the probe beam is absorbed strongly at the nodes and almost transmitted at the antinodes. On the other hand, the dispersion within the EIT window is positive to the probe beam at the nodes but negative at the antinodes, or vice versa, as shown by the red dashed lines in these figures. This feature may open the possibility of a phase modulation across the probe beam [17].

Given that $n = \sqrt{1+\chi} \approx 1 + \chi/2$, $\chi = \chi' + i\chi''$, and $n = n_0 + n_{\text{R}} + in_{\text{I}}$, the real (dispersion) and imaginary (absorption) components of the refractive index are written, respectively, as $n_{\text{R}} = \chi'/2$ and $n_{\text{I}} = \chi''/2$, where n_0 is the background index of the atomic medium. With the spatially modulated coupling intensity, n_{R} and n_{I} behave as periodic functions of (x, y), as shown, respectively, in Figs. 2(d) and 2(e). Such modulated index profiles clearly indicate the formation of a 2D optically induced atomic lattice. Under the slowly varying approximation, the propagation of the probe beam in the atomic medium is governed by the following Schrödinger-type equation:

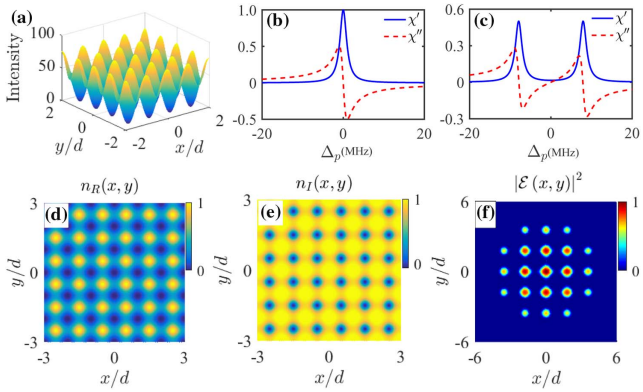

Fig. 2. (a) Periodical modulation of the effective coupling field due to the four-beam interference pattern with $\Omega_c = 2\pi \times 6$ MHz. (b), (c) Absorption and dispersion spectra at the nodes and antinodes of the periodic field, with $\Delta_c = 0$ MHz and $\gamma_{21} = \gamma_{32} = 1$ MHz. (d), (e) Spatially modified real (n_R) and imaginary (n_I) parts of the refractive index modulation, with $\Omega_c = 2\pi \times 6$ MHz, $\Delta_p = 0$ MHz, and $\Delta_c = 10$ MHz. (f) Numerical simulation of the intensity image of the probe beam's output, with the same parameters as those in (d), (e).

$$i\frac{\partial \mathcal{E}}{\partial z} = -\frac{1}{2k_0 n_0}\nabla_\perp^2 \mathcal{E} - k_0 \Delta n(x,y)\mathcal{E}, \tag{2}$$

where $\mathcal{E}$ is the electric field envelope of the probe beam, $\nabla_\perp^2 = \partial^2/\partial x^2 + \partial^2/\partial y^2$ is the transverse Laplacian, $\Delta n(x,y) = n_R + in_I$ is the "effective potential" induced by the effective coupling field according to Eq. (1), and $k_0 = 2\pi/\lambda_p$. By eliminating the transverse term, the transmission function of the probe field at $z = L$ can be calculated analytically using Eq. (2) and is given by $T(x,y) = \mathcal{E}_p(x,y,0)e^{-k_0 L\chi''/2}e^{ik_0 L\chi'/2}$ [17]. In Fig. 2(f), we numerically simulate the 2D diffraction pattern by using beam a propagation method [19]. It can be seen that a weak Gaussian probe beam will be diffracted into a periodic pattern after propagating in such a 2D optical lattice.

Figure 3 shows the experimental observation of the output intensities of a weak Gaussian probe beam. In the absence of the coupling beams, the output of the probe beam still remains Gaussian with normal diffraction, as shown in Fig. 3(a). When turning on the two coupling beams in the x–z and y–z planes, respectively, a stripe pattern appears in the outputs of the probe beam, as shown in Figs. 3(b) and 3(c). This is because discrete diffraction occurs when the probe beam passes through the optical lattice induced by the interference of the coupling beams. When the four coupling beams are present simultaneously, a square lattice pattern appears in the output of the probe beam, as shown in Fig. 3(d).

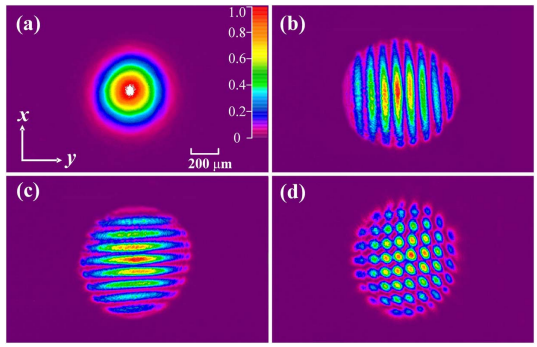

Fig. 3. Detected image profile of a weak Gaussian probe beam through the cell. (a) Output of the Gaussian pattern without the coupling beams. (b), (c) Outputs of the strip pattern in x and y directions, respectively. (d) Output of the 2D discrete diffraction pattern in the x–y plane. The powers of each coupling beam and the probe beam are given, respectively, by 16.0 mW and 3.0 mW, and the two-photon detuning $\Delta = \Delta_p - \Delta_c = 20$ MHz.

According to Eqs. (1) and (2), the refractive index can be controlled by system parameters, such as the power of the effective coupling field and the frequency detunings. This means that the diffraction pattern can also be manipulated by these tunable parameters. Figure 4 is the observed diffraction patterns with the different powers of the coupling laser. For a weak coupling laser ($P = 4$ mW), the diffraction intensity is weak, as shown in Fig. 3(a). With increasing power, the diffraction pattern gradually becomes strong, as shown in Figs. 4(b) and 4(c). When the power increases to 16 mW [Fig. 4(d)], the diffraction pattern can be clearly seen. This is within our expectation because as the power increases, the EIT effect gradually opens up the individual antinodes, making more light available for diffraction. However, with further increasing power, a strong coupling field renders the majority part of one period of the lattice transparent, and thus the visibility of the diffraction pattern is reduced, as shown in Figs. 4(e) and 4(f). Such a wide opening period concentrates the light on the forward direction and limits the chances of light to stray into the higher order.

Figure 5 is the observed diffraction patterns of the probe beam for the different two-photon detunings $\Delta = \Delta_p - \Delta_c$, when the frequency detuning of the probe beam is fixed at $\Delta_p = 0$. It can be seen that the clearest and brightest diffraction pattern is obtained when $\Delta = 20$ MHz, as shown in Fig. 5(d). As Δ moves far away from this optimal point [Figs. 5(a) and 5(f) with $\Delta = -10$ and 40 MHz, respectively], the dispersion is weakened, and thus the resolution of the diffraction pattern becomes much weaker. When $\Delta = 0$ [Fig. 5(b)], a simple inspection of Eq. (1) reveals that the real part of the susceptibility vanishes, and a 2D optical lattice with pure amplitude modulation is formed. On the other hand, in the non-resonant case ($\Delta \neq 0$), both phase ($\chi' \neq 0$) and amplitude ($\chi'' \neq 0$) modulations are introduced to adjust the probe beam. It is observed that more energy of the probe beam is transferred to a higher

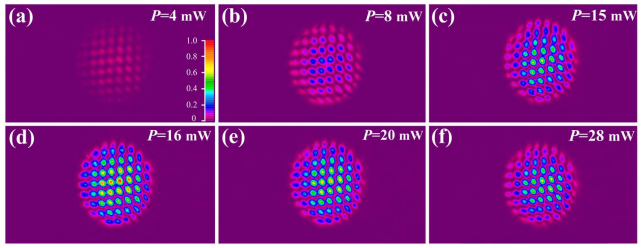

Fig. 4. Experimentally observed diffraction patterns of a weak Gaussian probe beam propagating through 2D optical lattice with the different powers of each coupling beam. (a) $P = 4$ mW, (b) $P = 8$ mW, (c) $P = 15$ mW, (d) $P = 16$ mW, (e) $P = 20$ mW, and (f) $P = 28$ mW. The other experimental parameters are the same as those in Fig. 3.

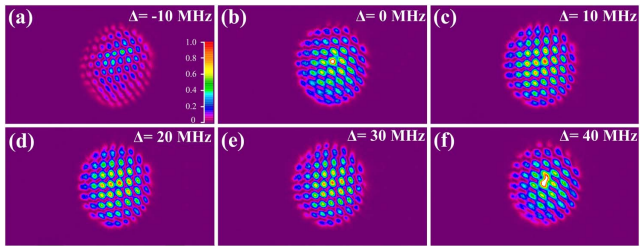

Fig. 5. Experimentally observed diffraction patterns of a weak Gaussian probe beam propagating through 2D optical lattice with different two-photon detunings. (a) $\Delta = -10$ MHz, (b) $\Delta = 0$ MHz, (c) $\Delta = 10$ MHz, (d) $\Delta = 20$ MHz, (e) $\Delta = 30$ MHz, and (f) $\Delta = 40$ MHz. The other experimental parameters are the same as those in Fig. 3.

diffraction pattern in such a hybrid lattice [Figs. 5(c)–5(e)] than that in the pure amplitude lattice [Fig. 5(b)].

It should be noted that the period or lattice constant of the 2D atomic lattice can be, in principle, adjusted by varying the angle between the coupling beams. However, the Doppler effect due to the ballistic or diffusive behaviors of moving thermal atoms will hinder the observation of the diffraction pattern. In our experiment, we adopt this small-angle paraxial arrangement ($\theta \approx \theta' \approx 0.2°$) to suppress the severe Doppler effect and observe a more discrete diffraction pattern. In addition, increasing the temperature of the Rb cell can effectively enhance the atomic density and can thus generate a larger refractive index constant. Here, the temperature is controlled at about 377 K with an atomic density of $\sim 7.68 \times 10^{12}$ cm^{-3}. In addition to the square lattice, other types of complex lattice structures, such as honeycomb lattice, kagome lattice, and Lieb lattice, can also be constructed in the current system by choosing an appropriate configuration of lasers.

In conclusion, we have experimentally realized a 2D optically induced atomic lattice in a coherently prepared three-level ^{85}Rb atomic medium inside a vapor cell. The changes in the discrete diffraction patterns of this 2D lattice under different coupling laser intensities and two-photon detunings have also been investigated. We have found that there are optimal conditions for the observation of diffraction patterns. Our work may pave the way for studying not only the control of light based on the periodically modulated medium, but also studying interesting physics, such as optical solitons [30], electromagnetically induced Talbot effect [33], and parity-time-symmetric related phenomena [34,35].

Funding. National Key RD Program of China (2017YFA0304203); National Natural Science Foundation of China (11674200, 61575116, 61705122, 61875112, 91736209); Program for Sanjin Scholars of Shanxi Province; Applied Basic Research Project of Shanxi Province (201701D221004); Key Research and Development Program of Shanxi Province for International Cooperation (201803D421034); 1331KSC.

REFERENCES

1. J. D. Joannopoulos, S. G. Johnson, J. N. Winn, and R. D. Meade, *Photonic Crystals: Molding the Flow of Light* (Princeton University, 2008).
2. D. N. Christodoulides, F. Lederer, and Y. Silberberg, Nature **424**, 817 (2003).
3. I. L. Garanovich, S. Longhi, A. A. Sukhorukov, and Y. S. Kivshar, Phys. Rep. **518**, 1 (2012).
4. X. Hu, Y. Liu, J. Tian, B. Cheng, and D. Zhang, Appl. Phys. Lett. **86**, 121102 (2005).
5. X. Zhang and Z. Liu, Nat. Mater. **7**, 435 (2008).
6. J. D. Teufel, T. Donner, M. A. Castellanos-Beltran, J. W. Harlow, and K. W. Lehnert, Nat. Nanotechnol. **4**, 820 (2009).
7. L. Lu, J. D. Joannopoulos, and M. Soljačič, Nat. Photonics **8**, 821 (2014).
8. T. Ozawa, H. M. Price, A. Amo, N. Goldman, M. Hafezi, L. Lu, M. C. Rechtsman, D. Schuster, J. Simon, O. Zilberberg, and I. Carusotto, Rev. Mod. Phys. **91**, 015006 (2019).
9. M. D. Leistikow, A. P. Mosk, E. Yeganegi, S. R. Huisman, A. Lagendijk, and W. L. Vos, Phys. Rev. Lett. **107**, 193903 (2011).
10. S. E. Han, A. Stein, and D. J. Norris, Phys. Rev. Lett. **99**, 053906 (2007).
11. A. Szameit, I. L. Garanovich, M. Heinrich, A. A. Sukhorukov, F. Dreisow, T. Pertsch, S. Nolte, A. Tünnermann, S. Longhi, and Y. S. Kivshar, Phys. Rev. Lett. **104**, 223903 (2010).
12. F. Lederer, G. I. Stegeman, D. N. Christodoulides, G. Assanto, M. Segev, and Y. Silberberg, Phys. Rep. **463**, 1 (2008).
13. P. Longo, P. Schmitteckert, and K. Busch, Phys. Rev. Lett. **104**, 023602 (2010).
14. M. S. Kang, A. Butsch, and P. S. J. Russell, Nat. Photonics **5**, 549 (2011).
15. D.-W. Wang, H.-T. Zhou, M.-J. Guo, J.-X. Zhang, J. Evers, and S.-Y. Zhu, Phys. Rev. Lett. **110**, 093901 (2013).
16. M. Fleischhauer, A. Imamoglu, and J. P. Marangos, Rev. Mod. Phys. **77**, 633 (2005).
17. H. Y. Ling, Y.-Q. Li, and M. Xiao, Phys. Rev. A **57**, 1338 (1998).
18. C. Li, T. Zhou, Y. Zhai, X. Yue, J. Xiang, S. Yang, W. Xiong, and X. Chen, Phys. Rev. A **95**, 033821 (2017).
19. J. Sheng, J. Wang, M.-A. Miri, D. N. Christodoulides, and M. Xiao, Opt. Express **23**, 19777 (2015).
20. J. Yuan, Y. Li, S. Li, C. Li, L. Wang, L. Xiao, and S. Jia, Laser Phys. Lett. **14**, 125206 (2017).
21. Z. Zhang, J. Feng, X. Liu, J. Sheng, Y. Zhang, Y. Zhang, and M. Xiao, Opt. Lett. **43**, 919 (2018).
22. Z. Zhang, X. Liu, D. Zhang, J. Sheng, Y. Zhang, Y. Zhang, and M. Xiao, Phys. Rev. A **97**, 013603 (2018).
23. J. Yuan, C. Wu, Y. Li, L. Wang, Y. Zhang, L. Xiao, and S. Jia, Opt. Express **27**, 92 (2019).
24. D.-W. Wang, H. Cai, L. Yuan, S.-Y. Zhu, and R.-B. Liu, Optica **2**, 712 (2015).
25. H. Cai, J. Liu, J. Wu, Y. He, S.-Y. Zhu, J.-X. Zhang, and D.-W. Wang, Phys. Rev. Lett. **122**, 023601 (2019).
26. M. C. Rechtsman, J. M. Zeuner, Y. Plotnik, Y. Lumer, D. Podolsky, F. Dreisow, S. Nolte, M. Segev, and A. Szameit, Nature **496**, 196 (2013).
27. Y. Zhang, Z. Wu, M. R. Belić, H. Zheng, Z. Wang, M. Xiao, and Y. Zhang, Laser Photon. Rev. **9**, 331 (2019).
28. Z. Zhang, F. Li, G. Malpuech, Y. Zhang, O. Bleu, S. Koniakhin, C. Li, Y. Zhang, M. Xiao, and D. D. Solnyshkov, Phys. Rev. Lett. **122**, 233905 (2019).
29. J. W. Fleischer, M. Segev, N. K. Efremidis, and D. N. Christodoulides, Nature **422**, 147 (2003).
30. Y. Zhang, Z. Wang, Z. Nie, C. Li, H. Chen, K. Lu, and M. Xiao, Phys. Rev. Lett. **106**, 093904 (2011).
31. F. Wen, H. Ye, X. Zhang, W. Wang, S. Li, H. Wang, Y. Zhang, and C. W. Qiu, Photon. Res. **5**, 676 (2017).
32. J. Sheng, M.-A. Miri, D. N. Christodoulides, and M. Xiao, Phys. Rev. A **88**, 041803 (2013).
33. J. Wen, S. Du, H. Chen, and M. Xiao, Appl. Phys. Lett. **98**, 081108 (2011).
34. Z. Zhang, Y. Zhang, J. Sheng, L. Yang, M.-A. Miri, D. N. Christodoulides, B. He, Y. Zhang, and M. Xiao, Phys. Rev. Lett. **117**, 123601 (2016).
35. Z. Zhang, D. Ma, J. Sheng, Y. Zhang, Y. Zhang, and M. Xiao, J. Phys. B **51**, 072001 (2018).